Application to METIS study case (WP4)

Authors : Dr. Marco PAGANI (GEM), Thomas, Chartier and Anna, Rood

METIS - Contract Number: 945121

Project officer: Katerina PTACKOVA

Document title	Application to METIS study case (WP4)
Author(s)	Dr. Marco PAGANI, Thomas, Chartier and Anna, Rood
Number of pages	34
Document type	Deliverable
Work Package	WP4
Document number	D4.6
Issued by	GEM
Date of completion	2023-03-20 11:29:13
Dissemination level	Public

Summary

This document illustrates the approach used for the construction of the hazard model for the METIS test site and describes the results. In the development of this model methods described in D4.1 were applied. This model will be also used within following deliverables to demonstrate the use of some of the new methodologies proposed within WP4.

Approval

Date	By
2023-03-20 16:40:03	Dr. Marco PAGANI (GEM)
2023-03-20 16:45:07	Dr. Irmela ZENTNER (EDF)

Research & Innovation Action

NFRP-2019-2020

D4.6 - Preparation of the METIS study case (WP4) and application

Version N°3

Authors: Thomas Chartier (GEM), Anna Rood (GEM)

Disclaimer

The content of this deliverable reflects only the author's view. The European Commission is not responsible for any use that may be made of the information it contains.

Document Information

Grant agreement	945121
Project title	Methods And Tools Innovations For Seismic Risk Assessment
Project acronym	METIS
Project coordinator	Dr. Irmela Zentner, EDF
Project duration	1st September 2020 – 31st August 2024 (48 months)
Related work package	WP 4 – Seismic hazard
Related task(s)	Task 4.7: Application to METIS study and guidelines
Lead organisation	GEM
Contributing partner(s)	
Due date	31/10/2022
Submission date	
Dissemination level	X

History

Version	Submitted by	Reviewed by	Date	Comments
N°1	Thomas Chartier	Marco Pagani	19/09/2022	
N°2	Anna Rood	Marco Pagani	30/01/2023	
N°2	Anna Rood	Manuela Villani	08/02/2023	
N°2	Anna Rood	Irmela Zentner Gloria Senfaunte	27/02/2023	
N°3	Anna Rood		20/03/2023	Final

Table of Contents

List of figures

List of tables

Abbreviations and Acronyms

Acronym	Description
CS	Conditional Spectra
ESHM20	2020 update of the European Seismic Hazard Model
GMM	Ground-Motion Model
MFD	Magnitude Frequency Distribution
PGA	Peak Ground Acceleration
PSA	Probabilistic Safety Assessment
PSHA	Probabilistic Seismic Hazard Analysis
SA	Spectral Acceleration
UHS	Uniform Hazard Spectra
WP	Work Package

Summary

This report illustrates the seismic-source characterisation and ground-motion characterisation defined for the METIS case study site, located in central Italy.

The document focuses on the datasets, methods, and models utilized to construct the various components of the model.

In the last part of the document, hazard results are presented.

Keywords

PSHA, test-site, seismic-source characterisation

1. Preamble

The goal of the METIS project is to improve existing seismic risk assessment tools and methodologies for nuclear safety. Most of the resources in the four technical work packages are devoted to improving the current state of practice. In the context of the project, it was also deemed important to demonstrate the use of the proposed methods and tools in a real application to a nuclear facility. The candidate facility initially selected for this demonstrative exercise was the Zaporizhzhia Nuclear Power Plant (ZNPP), Ukraine. The main points in favour of this site were its geographical location in Europe, access to a recent seismic hazard model through organisations already part of the METIS consortium, and information on the characteristics of the structure and various components of the plant.

During the initial part of the project, a more careful examination of the available ZNPP data revealed the unavailability of the input files describing the Probabilistic Seismic Hazard Analysis (PSHA) input model. This data unavailability combined with the exceptionally low level of seismic hazard at the site, caused the use of the ZNPP site to be reconsidered and other candidate sites to be examined. Instead, a hybrid-site option was suggested in which a hypothetical ZNPP-like nuclear installation exists on the western coast of Tuscany, Italy.

Due to the lack of a site-specific seismic hazard study for this new hybrid site, the GEM Foundation, the organization tasked to produce a seismic hazard model in the METIS project, decided to develop a simple hazard model that could be used to characterise the expected level of shaking. For this task, the members of the METIS External Advisory Board proposed to follow the Recommendations of the Senior Seismic Hazard Analysis Committee (SSHAC, 1997; 2012) or at least to endorse the principles of the SSHAC recommendations.

The GEM hazard team, while recognizing the authoritativeness of the SSHAC Guidelines, opted for a simpler approach which sought for feedback and comments from the members of the consortium but did not imply a formal participatory peer review process, which is one distinctive aspect of the SSHAC process. We consider this option acceptable in the context of a research project like METIS where there is no need to comply with any specific regulatory requirement.

2. Introduction

A key prerequisite to seismic probabilistic safety assessment (PSA) for nuclear safety is the analysis of the seismic hazard at the site of the nuclear facility. WP4 of the METIS project aims to develop new approaches and tools for the calculation of seismic hazard, and the application of these methodologies to the METIS case study site.

This report focuses on the seismic-source characterisation component of seismic hazard analysis, which aims to define the locations, geometries, magnitudes, and rates of occurrence of earthquakes of engineering importance for METIS case study. This includes a hypothetical nuclear facility located along the western coast of Tuscany, Italy, in proximity of Orbetello, which is one of the areas with the lowest levels of seismic hazard in Italy.

In this document, we provide a description of the datasets, methods, and models used to develop the seismic-source characterisation. Due to limitations in data and knowledge, in the seismic-source characterisation, we model epistemic uncertainties by defining alternative methods or parameters in a logic tree framework. Specifically, alternative logic tree branches are included for the earthquake declustering model, the maximum earthquake magnitude, the magnitude frequency distribution (MFD), and the seismicity smoothing parameters.

Finally, ground-motion models appropriate for the METIS case study site are combined with the seismic-source characterisation to calculate seismic hazard results for the METIS case study site. Section 3 provides an illustrative description of the ground-motion models adopted for the analysis of seismic hazard. In this document we describe some of the more traditional hazard results leaving for further analyses the calculation of more specific products.

1.1. Scope of project

Guidelines for conducting PSHA for sites hosting critical infrastructures, such as nuclear facilities, are provided by the Senior Seismic Hazard Analysis Committee (SSHAC, 1997; 2012). These guidelines provide a formal, structured methodology to warrant reasonable regulatory assurance that the centre, body, and range of technically defensible interpretations have been adequately captured. The complete characterisation of uncertainty in present-day technical knowledge, available data, methods, and models is required to provide reproducible, defensible, transparent, and stable ground-motion estimates for these facilities. However, the rigor of the SSHAC methodology requires specific resources of many years and the collaboration of many teams of experts.

Importantly, the METIS case study site in central Italy is not the site of a nuclear facility, nor is it proposed to be one. The METIS case study site in central Italy was selected in WP3 as an appropriate site, with higher seismicity than the location of the Zaporizhzhya Nuclear Power Plant in Ukraine, to achieve the best compromise to

complete the objectives of WP4, 5, 6, and 7. Similarly, the complexity of the seismic-source characterisation developed here in WP4 simply needs to be sufficiently realistic for its use in the subsequent work packages.

1.2.   The OpenQuake Engine

An important objective of the METIS project is to develop open-source methods and tools, for greater transparency, collaboration, quality, and use in nuclear engineering practice. Therefore, various seismic hazard methods developed in this project were implemented in the OpenQuake suite.

The OpenQuake Engine is the open-source, community-driven seismic hazard and risk calculation software developed by the Global Earthquake Model (Pagani et al., 2014). The source code of the OpenQuake Engine is available on a public web-based repository accessible at the following address: http://github.com/gem/oq-engine.

To construct the seismic-source characterisation in this project, packages were used from the OpenQuake Model Building Toolkit (https://github.com/GEMScienceTools/oq-mbtk) and functionalities within the OpenQuake Hazard Modeller's Toolkit (https://github.com/gem/oq-engine/tree/master/openquake/hmtk).

2. Seismic-source characterisation

2.1.   Seismogenic sources

Components of the seismogenic-source model developed in the context of the 2020 update of the European Seismic Hazard Model (ESHM20) were used as a primary dataset to model the spatial and temporal distribution of seismicity in proximity to the METIS case study site in central Italy (Danciu et al., 2021). Specifically, we used the ESHM20 tectonic super zones (TECTO) model, which was developed to describe large geographical regions with internally consistent tectonics as zones of distributed seismicity (Figure 1).

Initially, a hazard analysis for the case study site was conducted using the ESHM20 area sources model (Danciu et al., 2021). However, limited seismicity has been recorded in each ESHM20 area source zone within the reference earthquake catalogues, particularly in the case study host zone. From a seismic-source characterisation perspective, this resulted in large uncertainties in the regression of the MFD for each zone. Therefore, we instead used the ESHM20 tectonic super zones model which was developed to obtain a more robust estimation of the MFD for each zone, given the larger number of earthquakes within each tectonic super zone relative to each area source zone.

The METIS case study site in central Italy is located within the ESHM20 tectonic super zone TSZ050. This super zone covers an area both onshore and offshore, and has an approximately rectangular geometry elongated in a NW-SE direction sub-parallel to the western coast of central Italy. It is important to note that the spatial pattern of seismicity within each tectonic super zone is preserved with our smoothing approach as described in Section 2.3.3.

2.2. The earthquake catalogue
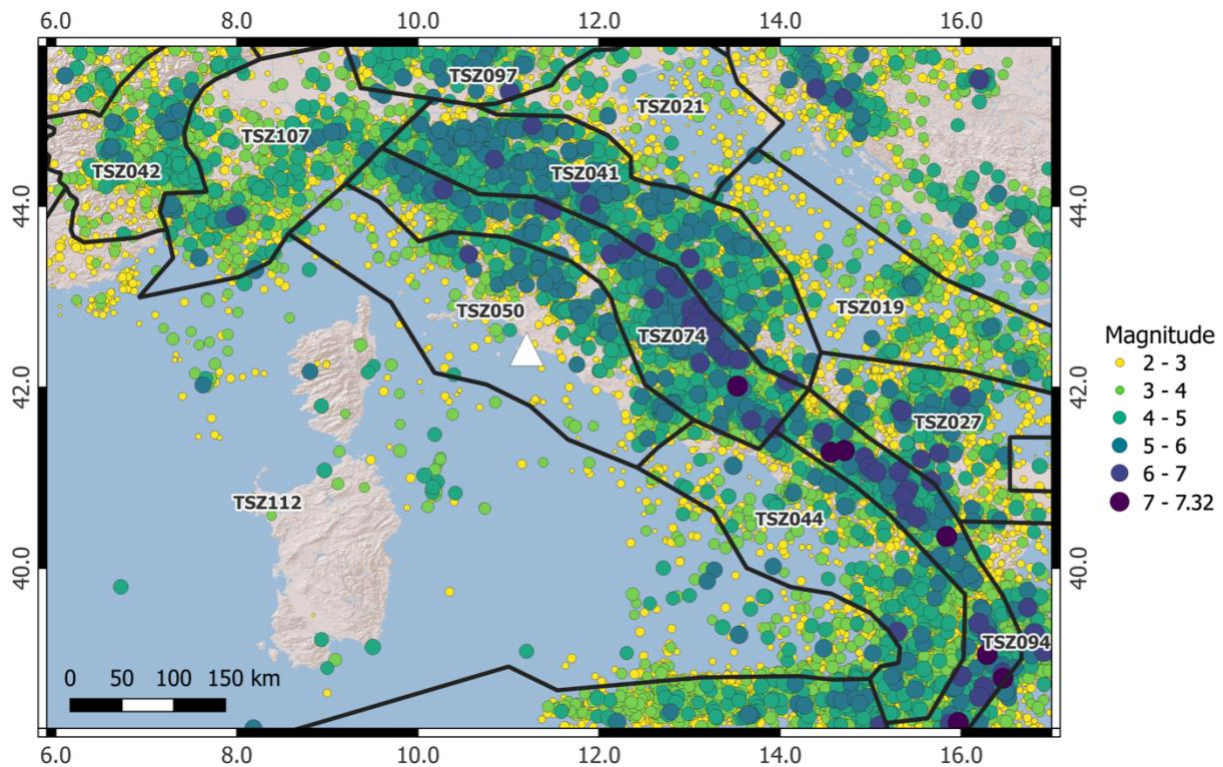
Figure 1: Map of the location of the METIS case study site in central Italy. The location of the case study site is indicated by the white triangle. The coloured circles are the epicentres contained in the earthquake catalogue, with the colour and size of the circle corresponding to the magnitude (Mw) of the earthquake. The black polygons are the ESHM20 tectonic super zones model labelled with the ESHM20 ID assigned to each super zone (Danciu et al., 2022).

The METIS case study lies in an area of low seismicity where information about active fault structures is not available (DISS Working Group, 2021). Therefore, for the construction of the earthquake occurrence model, historical earthquake data are relied on entirely. In Italy, this earthquake catalogue information is generally of high quality.

A homogeneous earthquake catalogue is a fundamental dataset for seismic hazard analysis. To achieve this goal, we combined information from two datasets including historical and instrumental earthquake information, respectively. For the years 1000-1959, the Parametric Catalogue of Italian Earthquakes (CPTI15 version 4; Rovida et al., 2022) was used. For the years 1960-present, all earthquakes greater than Mw 2.0 in the Homogenized Instrumental Seismic Catalog (HORUS) of Italy (Lolli et al., 2020) were used. Where "present" is the date of data access: 11th May 2022 (last earthquake is eventID 458713).

The catalogue obtained using these two datasets covers Italy and the surrounding regions (Figure 1) and contains 94347 earthquake events from the year 1000 to 2022. The earthquake magnitudes included in this catalogue range from Mw 2.0 to Mw 7.3,

where the Mw 7.3 event is associated with the 1693 Sicily earthquake. Each earthquake event in the catalogue records its date, time, location, hypocentral depth, and magnitude.
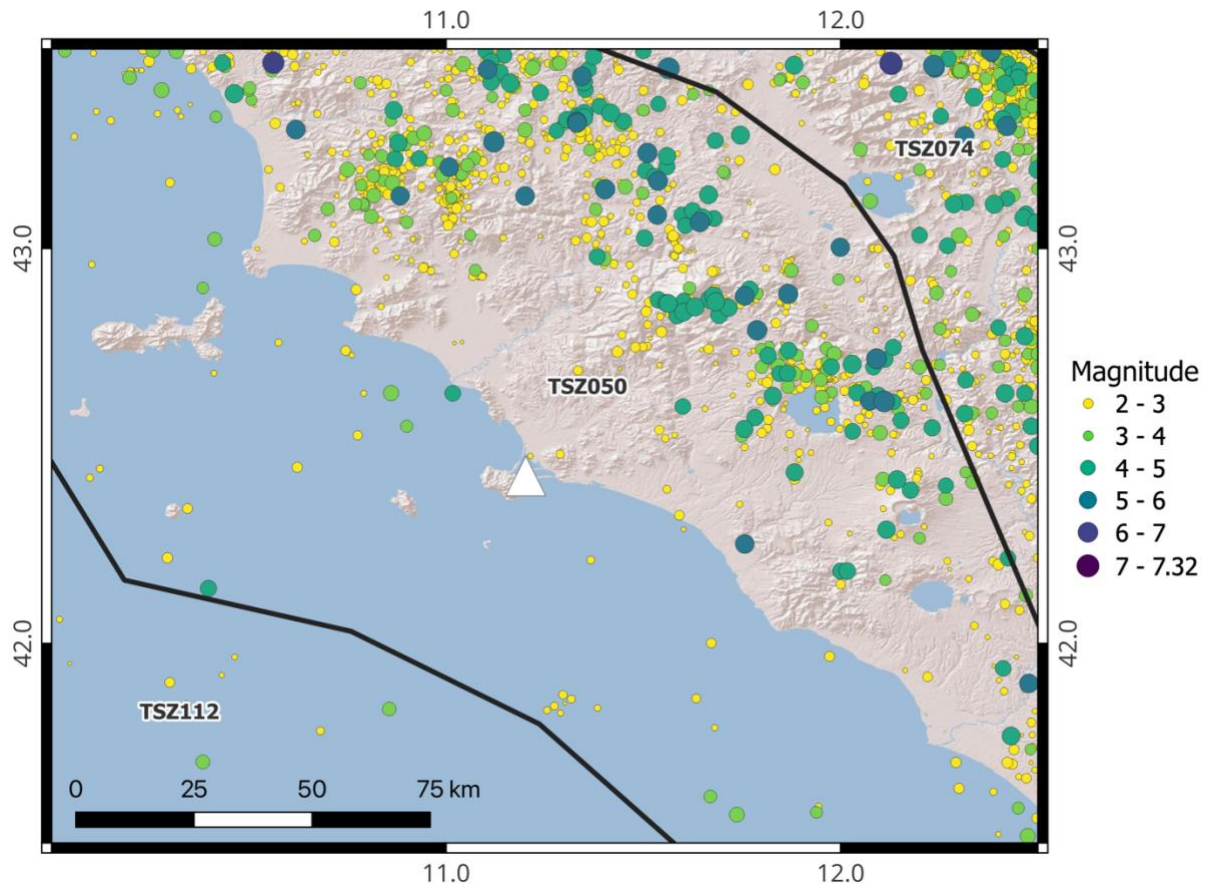

Figure 2: Map of the local seismicity around the METIS case study site. The location of the case study site is indicated by the white triangle. The coloured circles are the epicentres contained in the earthquake catalogue, with the colour and size of the circle corresponding to the magnitude (Mw) of the earthquake. The black polygons are the ESHM20 tectonic super zones model labelled with the ESHM20 ID assigned to each super zone (Danciu et al., 2022).

The super zone TSZ050 contains seismicity of moderate magnitude, which is mostly provided by the instrumental record. In zone TSZ050, there are 32 earthquake events in the catalogue greater than Mw 5.0. The >Mw 5.0 earthquake at the closest distance to the case study site is a Mw 5.1 earthquake that occurred approximately 50 km to the southeast of the site (Figure 2). There is only one >Mw 6.0 earthquake within the catalogue in zone TSZ050, which is a Mw 6.1 earthquake at approximately 130 km to the northeast of the site.
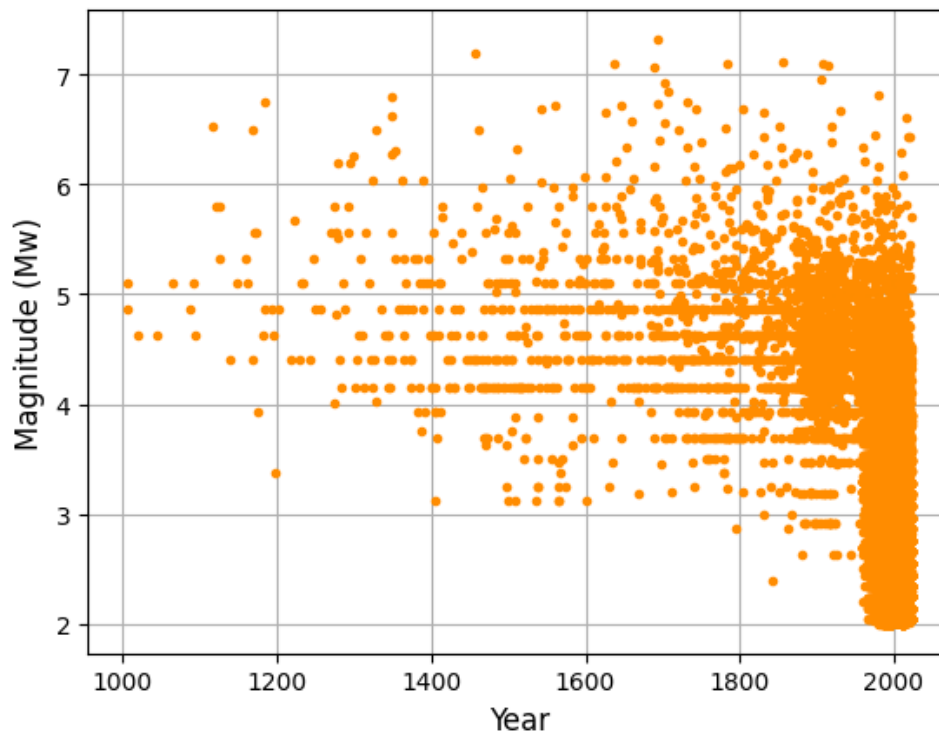
Figure 3: Magnitude-time plot of the declustered earthquake catalogue developed in this project. Each orange circle is an earthquake event recorded in the declustered catalogue. The higher density of points after 1960 is due to the instrumental HORUS catalogue being used after this date.

2.2.1. Catalogue declustering

Time-independent PSHA assumes that earthquake occurrence can be represented by a stationary Poisson process. However, earthquake catalogues contain events that cluster seismicity in space and time. Therefore, to only consider independent earthquake events within the earthquake catalogue, the catalogue was declustered by identifying and removing dependent earthquake events that occurred in clusters, such as foreshocks, aftershocks, and swarms. To achieve this declustering, we used the windowing algorithm of Knopoff and Gardner (1974), in which earthquakes within a certain space and time window of the mainshock are classified as dependent and so removed from the catalogue. Three different declustering space and time windows were used: Gardner and Knopoff (1974), Uhrhammer (1986), and Grünthal (1985). The declustered catalogues produced by the three different space and time windows were included in our seismic-source characterisation as three alternative logic tree branches.

The weights of the branches of the logic tree were defined using the Poissonian test developed in WP4.1 of the METIS project (see Chartier, 2022). The Poissonian test investigates the distribution of space-time distances between earthquakes events within a declustered catalogue compared to a synthetic Poissonian catalogue. Table 1 shows the results of the Poissonian test performed on the three declustered catalogues, in which a higher test score indicates that the catalogue is more similar to

a Poissonian catalogue. The Uhrhammer (1986) space and time window retained the largest number of earthquakes and received the highest score in the Poissonian test of the three declustering space and time windows. Therefore, the Uhrhammer logic tree branch was set a higher weight of 0.6 and the Gardner and Knopoff (1974) and Grünthal (1985) logic tree branches were both set a lower weight of 0.2.

Declustering space and time window	Poissonian test score	Total number of events retained	Number of events Mw≥5	Logic tree branch weight
Gardner and Knopoff 1974	0.435	32443	636	0.2
Uhrhammer 1986	0.583	52816	678	0.6
Grünthal 1985	0.426	20456	614	0.2

Table 1: Declustered catalogue results for the three declustering space and time windows.

2.2.2. Catalogue completeness

A catalogue completeness analysis is used to determine the earliest time at which all earthquake events for different magnitude bins are included in the catalogue. This analysis is necessary to obtain reliable seismicity rates from an earthquake catalogue, specifically so that the rate of occurrence of larger earthquakes is not overestimated and the rate of occurrence of smaller earthquakes is not underestimated. This is to say that the magnitude of completeness directly impacts the reliability of the b-value calculation in a Gutenberg-Richter MFD (Section 2.3.2).

For each super zone, many potential magnitude-time completeness windows were automatically calculated from Mw 3.0 to Mw 7.0 from the years 1700 to 2010. Visual analysis of the earthquakes contained within the declustered catalogue (Figure 3) was used to define magnitude-year combinations (i.e., earthquakes) that must be included or excluded by the completeness windows. We decided to discard the completeness windows that were including the following earthquakes: Mw 4.1 in 1959 and Mw 5.5 in 1875. and the ones that were excluding an earthquake of Mw 6.0 occurred in 1920. This reduced the number of potential completeness windows down to 790 windows that fulfilled these requirements (Figure 4).
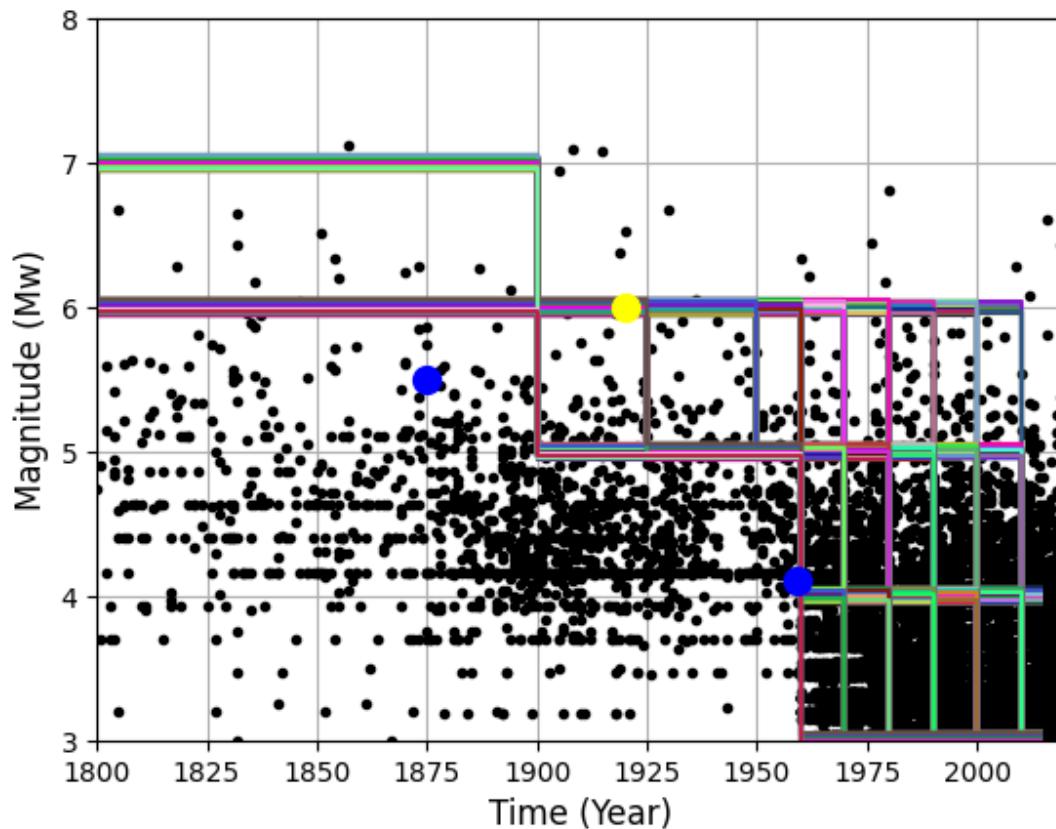
Figure 4: Automatically generated potential completeness windows. Each coloured line is one of 790 completeness windows that fulfil the constraint requirements. Blue circles are the magnitude-time combinations to be excluded and the yellow circle is the magnitude-time combination to be included. Black circles are the declustered earthquake catalogue events shown in Figure 3.

Source Zone	Magnitude (Mw)	Time (Year)
TSZ050	4.0	1990
	5.0	1900
	7.0	1800
TSZ074	4.0	2010
	5.0	2000
	6.0	1800

Table 2: Completeness windows results. Source zone TSZ050 hosts the METIS case study site. TSZ074 is a more distant, but more seismically active source zone located in the Apennines.

For each source zone, the final completeness windows were decided by an assessment of how well the resulting Gutenberg-Richter MFD matched the observed seismicity. For a given completeness window, the a-value and b-value of a Gutenberg-Richter MFD were calculated and the difference between the modelled MFD and observed seismicity was then computed. Subsequent iterations optimized the completeness windows to closest match the observed seismicity within the source zone. For example, for host zone TSZ050 the magnitude of completeness of the declustered catalogue is Mw 4.0 from 1990, Mw 5.0 from 1900, and Mw 7.0 from 1800 (Table 2, Figure 5). The completeness windows that were calculated for each source zone are more conservative, i.e., smaller, than both the historical and statistical completeness windows of Visini et al., (2022) for central Italy. However, this is expected due to the much larger area used by Visini et al., (2022) relative to our source zones.
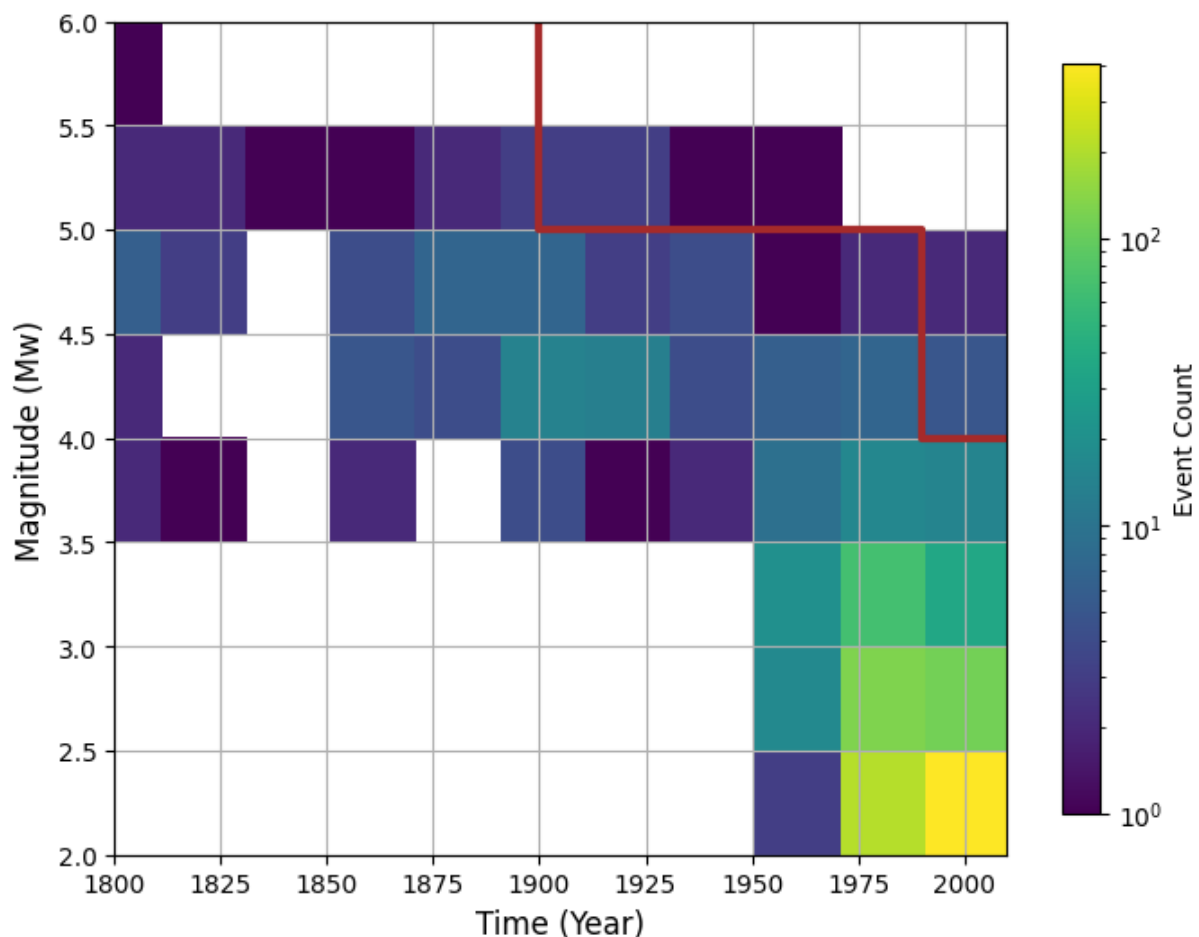
Figure 5: Magnitude-time density plot for declustered catalogue events in host zone TSZ050 with the optimized magnitude of completeness (red line).

2.3.   Distributed seismicity model

2.3.1. Maximum magnitude

The maximum magnitude (M_{max}) earthquake to be considered within each source zone was defined based on the maximum magnitude observed earthquake in each source zone ($M_{max-obs}$), from either the historical or instrumental component of our declustered catalogue. To account for the epistemic uncertainty of M_{max}, three values were considered, a lower bound $M_{max}1$, central estimate $M_{max}2$, and upper bound $M_{max}3$.

For $M_{max}1$, the $M_{max-obs}$ was simply used, with a value of Mw 6.0 assigned to any source zone with $M_{max-obs}$ < Mw 6.0. The assignment of this minimum limit of the maximum magnitude was to provide confidence that sufficiently large values of magnitude were admitted in every source zone even if the previously recorded events had relatively low values. A magnitude increment was then systematically added to $M_{max}1$, to provide $M_{max}2$, and then added again to provide $M_{max}3$. This magnitude increment addition between each M_{max} branch was to compensate for the short observation period of the catalogue relative to the length of the earthquake cycle.

The value of the magnitude increment depended on whether the source zone $M_{max}1$ was less than or greater than Mw 6.5. If the $M_{max}1$ value was less than Mw 6.5, then $M_{max}2$ was assumed to equal $M_{max}1$ plus a magnitude increment of 0.3, and $M_{max}3$ was assumed to equal $M_{max}1$ plus a magnitude increment of 0.6. This magnitude increment of 0.3 corresponds to the statistical uncertainty (i.e., standard deviation) of the magnitude in the ESHM20 earthquake catalogue. If the $M_{max}1$ value was greater than Mw 6.5, then $M_{max}2$ was assumed to equal $M_{max}1$ plus a magnitude increment of 0.2, and $M_{max}3$ was assumed to equal $M_{max}1$ plus a magnitude increment of 0.4. This lower magnitude increment was selected to prevent including magnitudes that may be too large for the source zone. The three M_{max} values of each source zone are shown in Figure 6.

A weight of 0.2 was assigned to the $M_{max}1$ logic tree branch, a weight of 0.6 was assigned to the $M_{max}2$ logic tree branch, and weight of 0.2 was assigned to the $M_{max}3$ logic tree branch, respectively (Table 3).

The M_{max} values for the host zone were modelled independently from the other source zones. $M_{max}1$ is the $M_{max-obs}$, with a weight of 0.2, $M_{max}2$ is $M_{max}1$ plus a magnitude increment of 0.3 with a weight of 0.6, and $M_{max}3$ is $M_{max}1$ plus a magnitude increment of 0.6 with a weight of 0.2. The host zone M_{max} values are provided in Table 3.

M_{max} branch	Zone M_{max}		Weight
	TSZ050	**TSZ074**	
$M_{max}1$	6.04	7.08	0.2
$M_{max}2$	6.34	7.28	0.6
$M_{max}3$	6.64	7.48	0.2

Table 3: Maximum magnitude (M_{max}) logic tree branch values and weights. Source zone TSZ050 hosts the METIS case study site. TSZ074 is a more distant, but more seismically active source zone located in the Apennines.
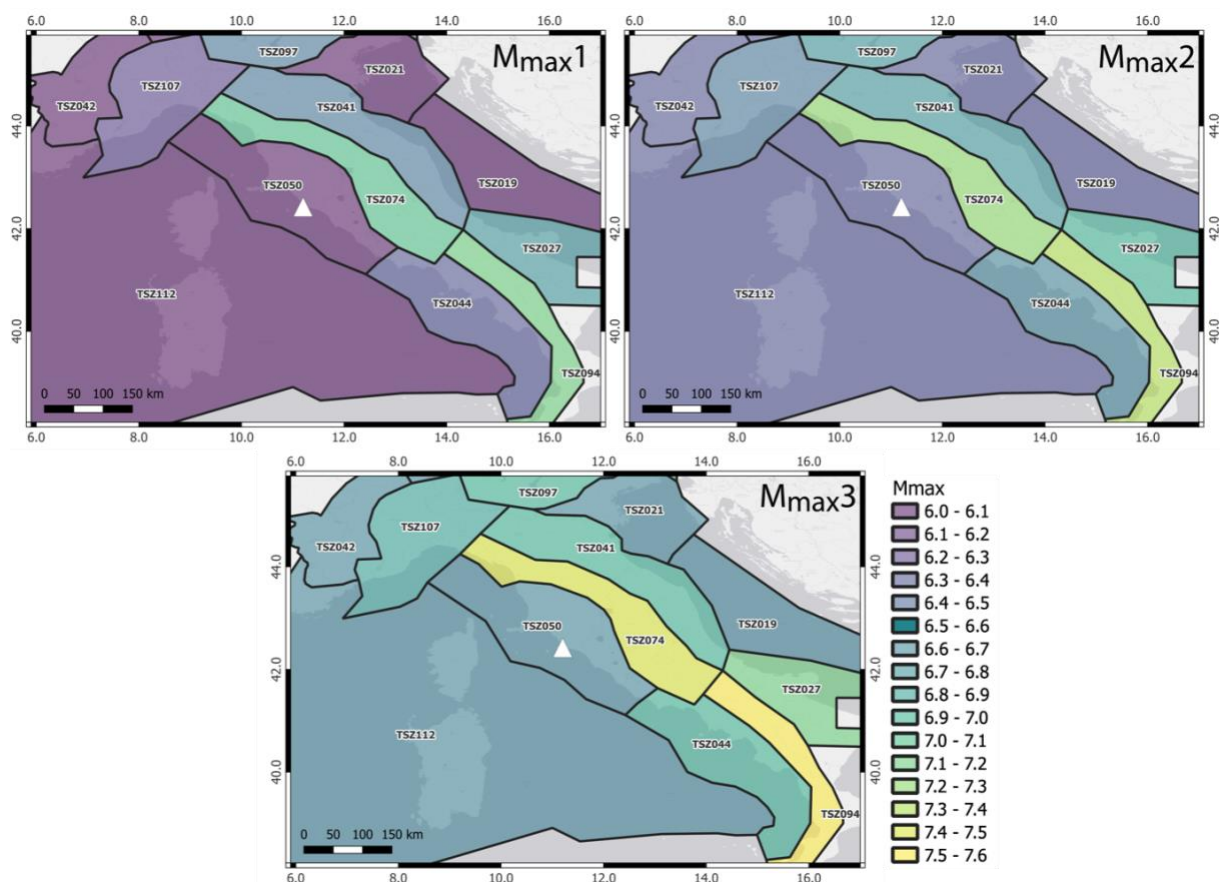

Figure 6: Three M_{max} values of each source zone. Note that the host zone TSZ050 M_{max} values are modelled separately in the seismic-source characterization logic tree.

2.3.2. Seismicity rates

A magnitude frequency distribution (MFD) for each source zone was modelled using the declustered catalogue (Section 2.2.1) and the optimized magnitude-time completeness windows (Section 2.2.2). The seismicity rates were computed as a double-truncated Gutenberg-Richter distribution with a magnitude binning interval of 0.1, a minimum magnitude of Mw 4, and a source-dependent maximum magnitude.

The Gutenberg-Richter a-value and b-value were calculated using the algorithm of Weichert (1980), which allows for the use of different observation periods for different earthquake magnitudes (Figure 7, Appendix A). To account for the epistemic uncertainty in the MFD of the host zone (TSZ050), not only the mean b-value was considered, but also a logic tree branch for plus and minus 1σ. These mean b-value was given a weight of 0.6 in the logic tree, and the mean b-value plus and minus 1σ branches were given a weight of 0.2.
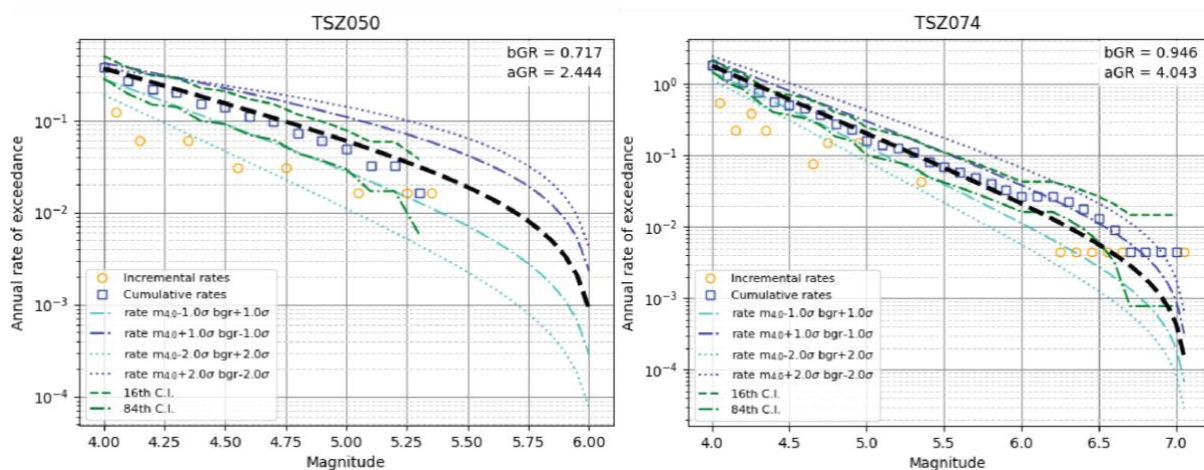
Figure 7: Magnitude frequency distribution (MFD) for the source zone TSZ050. Observed incremental (blue squares) and observed cumulative (red squares) rates are plotted and the mean modelled MFD is shown as the dashed green line.

The distribution of earthquake hypocentral depths in each source zone was assessed by normalizing the number of earthquake events in our declustered catalogue in three hypocentral depth ranges: 0-10 km, 10-20 km, and 20-35 km (Figure 8). The normalized count number in each depth bin was used to define the distribution. For example, it can be seen in Figure 8 that the host zone TSZ050 has a greater proportion of shallow earthquakes than deep ones.
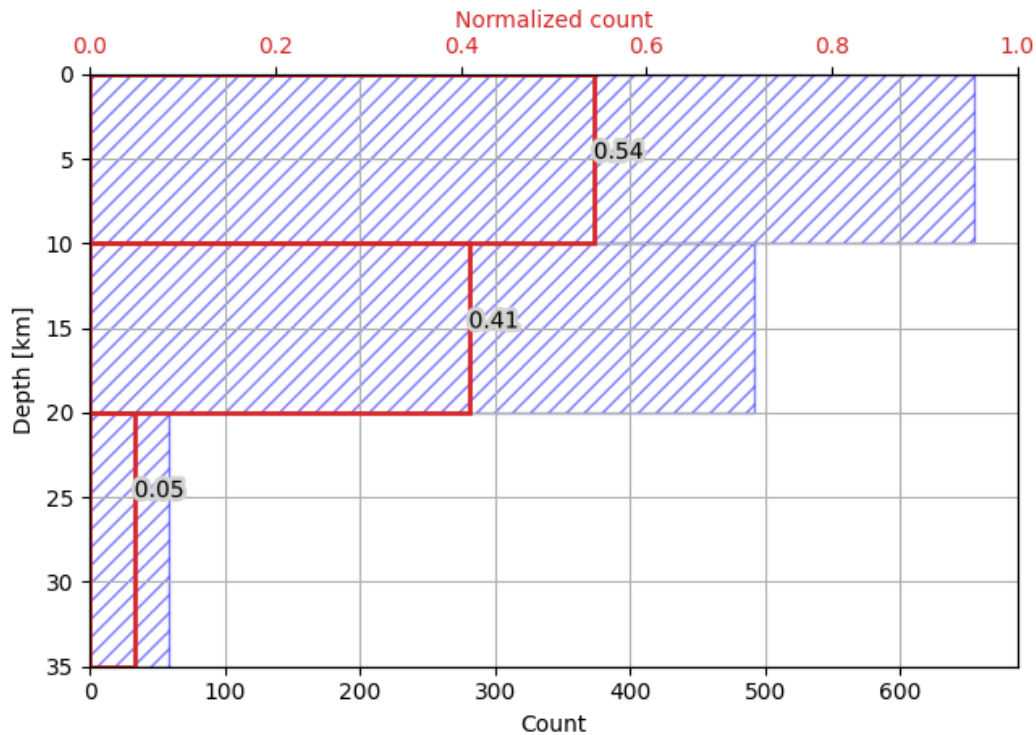
Figure 8: Hypocentral depth distribution of earthquakes in source zone TSZ050. Blue shaded area is the absolute earthquake event count in each hypocentral depth bin, and the red line is the normalized count.

A seismogenic depth of 0-30 km was used for all source zones. The magnitude-area fault scaling relationship for stable continental region of Leonard (2014), which was used in the ESHM20 for active crustal faults, was used for all source zones. For simplicity, four equally weighted nodal planes were applied to all source zones. Nodal plane 1: dip="60.0", rake="-90.0" and strike="60.0". Nodal plane 2: dip="60.0", rake="-90.0", and strike="120.0". Nodal plane 3: dip="60.0", rake="-90.0", and strike="0.0". Nodal plane 4: dip="90.0", rake="0.0", and strike="0.0".

2.3.3. Smoothing model

The ESHM20 super zones source model defines zones with internally consistent tectonics; however, it can be seen in Figure 1 that seismicity does not uniformly cover each source zone. Therefore, the earthquake catalogue was used to impart local variation in the distributed seismicity within each source zone.

Seismicity was spatially distributed within each source zone using a spatial kernel approach, incorporating methods similar to the one proposed by Frankel (1995). First, a Gaussian smoothing kernel was applied to the declustered earthquake catalogue for each source zone. Then, each source zone was defined as an evenly-spaced grid of points and the number of earthquakes in the Gaussian filtered catalogue associated to each grid node was counted. The fraction of earthquakes at each grid node was

combined with the MFD computed for the source zone to produce a grid of point-by-point earthquake occurrence rates (Figure 9).

Three sets of smoothing kernel parameters were included as logic tree branches in our seismic-source characterisation: Set 1, Set 2, and Set 3. In all three sets, smoothing kernel widths of 20 km, 40 km, and 60 km were used, and the relative weights of each kernel width was varied (Table 4). The relative weight assigned to each kernel width controls the strength of smoothing, such that a higher weight assigned to the kernel with a shorter width implies that the seismicity is kept closer to the nodes and vice-versa. This is visually demonstrated in Figure 9, as the modelled seismicity is most concentrated and most closely follows the patterns of the observed seismicity when using the Set 1 parameters. All three sets of smoothing kernel parameters have equally weight logic tree branch weights.

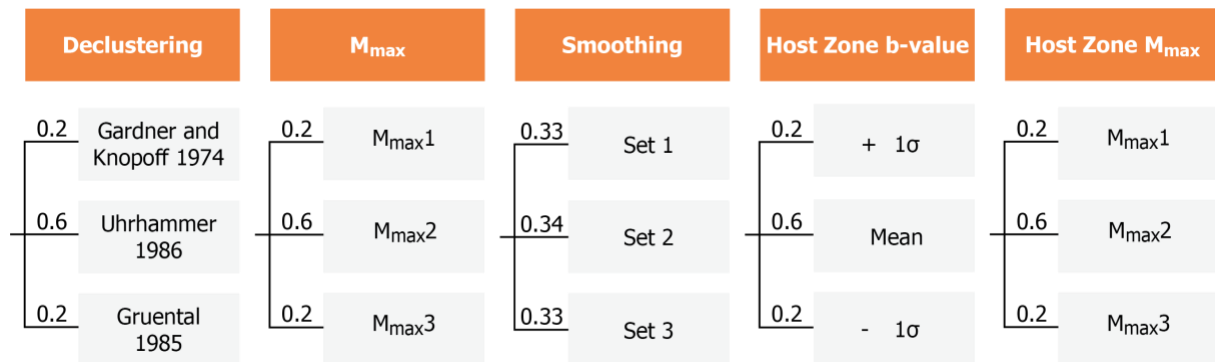|		Kernel width		
		20 km	40 km	80 km
Smoothing parameters	**Set 1**	0.90	0.07	0.03
	Set 2	0.80	0.15	0.05
	Set 3	0.60	0.30	0.10

Table 4: Smoothing kernel widths and weights of the three smoothing sets.
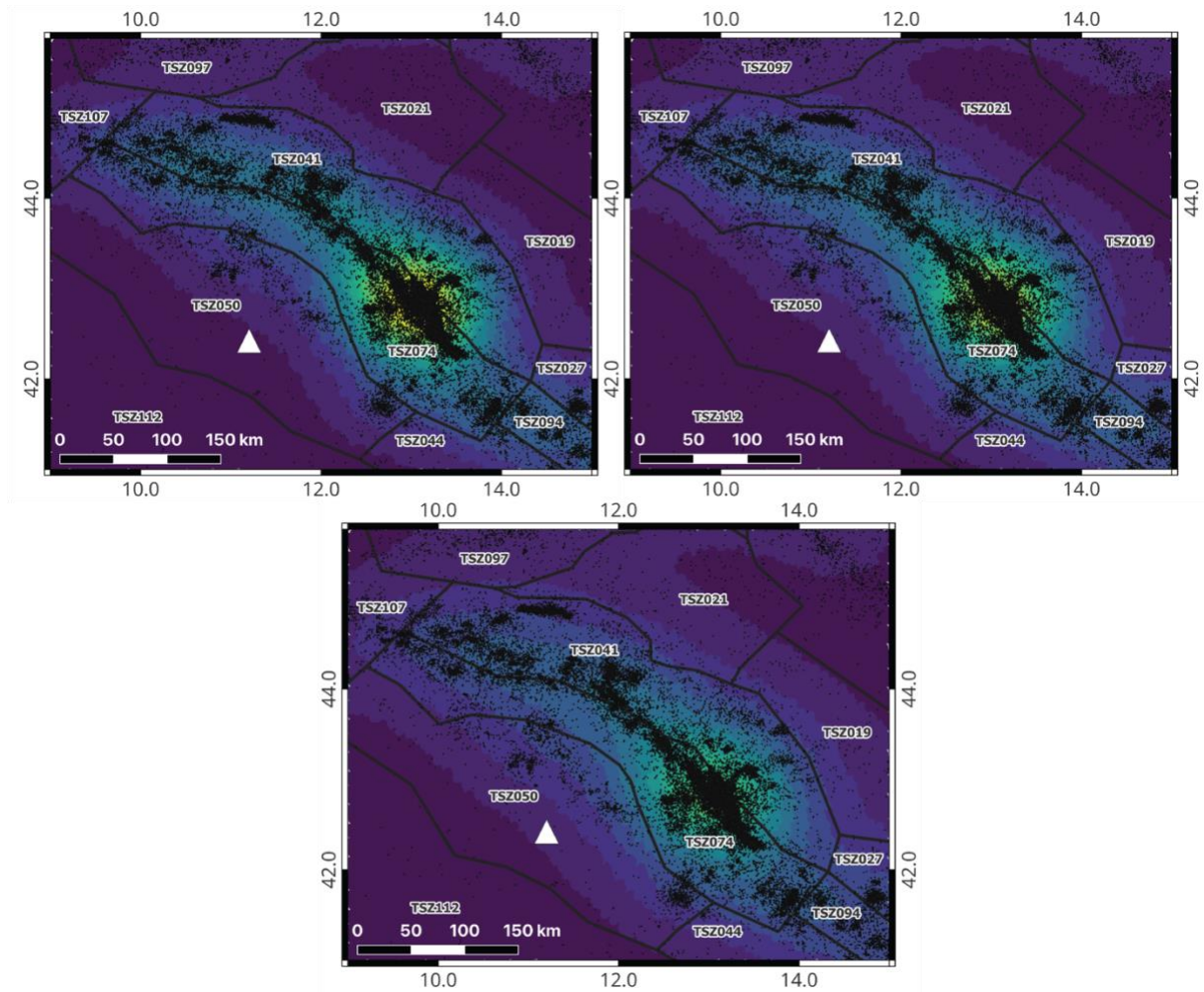
Figure 9: Impact of the smoothing kernel on the spatial distribution of the modelled seismicity. The recorded seismicity is shown as black points. Top left: Set 1, Top right: Set 2, Bottom: Set 3 (Table 4). Yellow to dark blue seismicity shows a decreasing number of earthquake occurrences at each node.
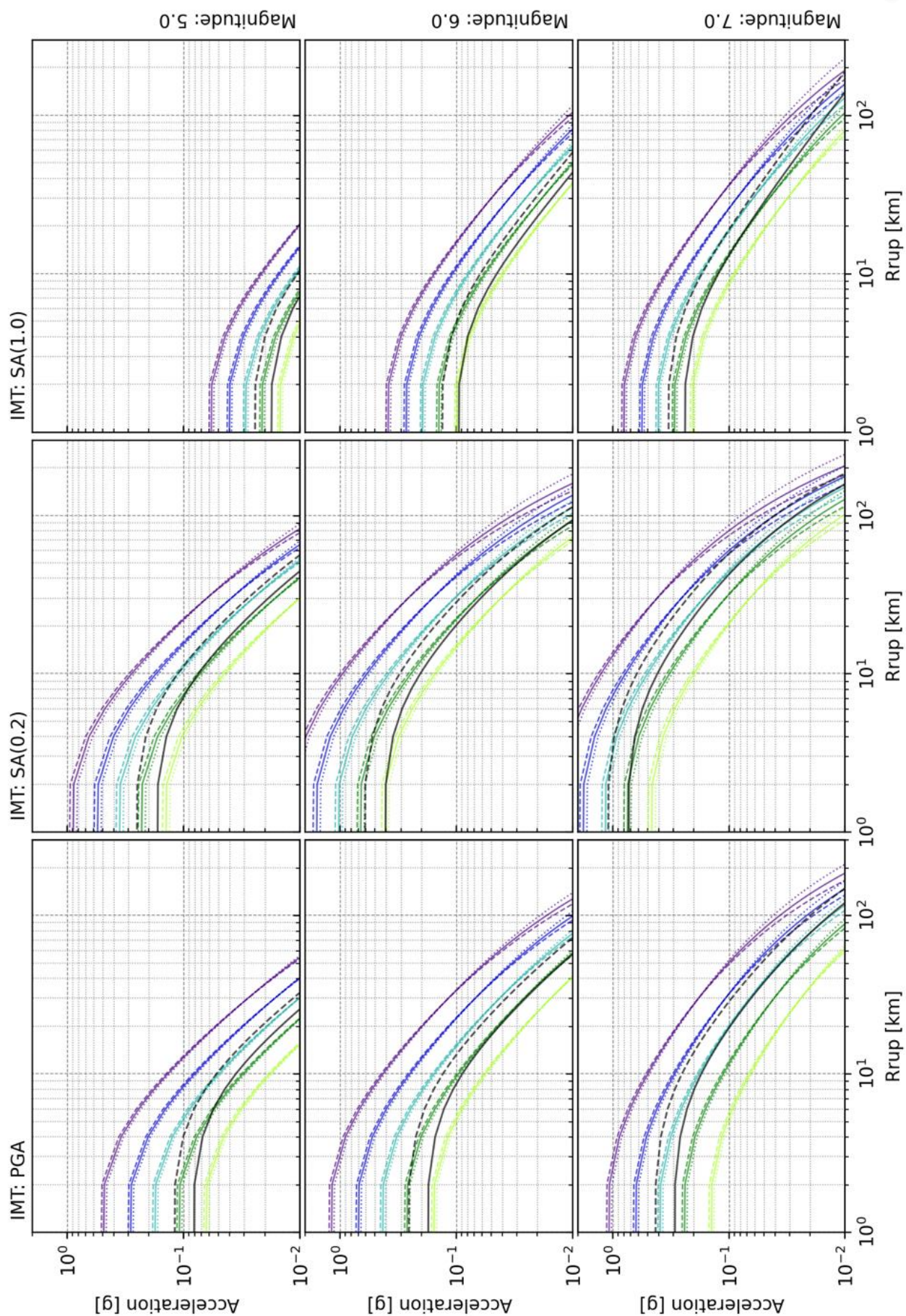
3. Logic tree

For this hazard analysis, we used the seismic-source logic tree presented in Figure 10. Overall, this logic tree has five branching sets, each once containing three alternative branches. Therefore, there are 125 alternative calculation paths through the seismic-source logic tree.

Declustering		M_{max}		Smoothing		Host Zone b-value		Host Zone M_{max}	
0.2	Gardner and Knopoff 1974	0.2	$M_{max}1$	0.33	Set 1	0.2	+ 1σ	0.2	$M_{max}1$
0.6	Uhrhammer 1986	0.6	$M_{max}2$	0.34	Set 2	0.6	Mean	0.6	$M_{max}2$
0.2	Gruental 1985	0.2	$M_{max}3$	0.33	Set 3	0.2	- 1σ	0.2	$M_{max}3$

Figure 10: Seismic-source characterisation logic tree developed in this project. The weight assigned to each branch is shown on the line leading to each alternative model or parameter. Note that the host zone is TSZ050.

For the ground-motion logic tree, two ground-motion models (GMMs) were used with equal weights, i.e., both have a weight of 0.5. The first GMM used in the logic tree is the scaled backbone ground-motion logic tree developed for the ESHM20, adapted from Kotha et al., (2020) by Weatherill et al., (2020). This GMM has five logic tree branches for alternative source stress parameters and three logic tree branches for alternative anelastic attenuation. The second GMM used is the Lanzano et al., (2019) GMM derived for Italy, modified to include the reference rock correction factor of Lanzano et al., (2022). For the site parameters required by the GMMs, the value of the average shear-wave velocity in the upper 30 m (V_{S30}) was set to 1000 m/s, to correspond with the Eurocode 8 rock category A (CEN, 2004). To account for high-frequency attenuation at this hard rock site, a site-specific zero distance kappa (k_0) of 0.025 s was used, which is the representative value for the reference rock sites in Italy determined by Lanzano et al., (2022). We accounted for epistemic uncertainty in this value for k_0 by including three alternative branches in our ground-motion logic tree. The branch for k_0=0.025 s was given a weight of 0.6, and two alterative k_0 branches for 0.01 s and 0.04 s, which are the alternative k_0 values investigated by Lanzano et al., (2022), were both given weights of 0.2.

| Kotha et al., 2020 - VLowStress,FastAtten	Kotha et al., 2020 - MidStress,FastAtten	Kotha et al., 2020 - VHighStress,FastAtten
Kotha et al., 2020 - VLowStress,MidAtten	Kotha et al., 2020 - MidStress,MidAtten	Kotha et al., 2020 - VHighStress,MidAtten
Kotha et al., 2020 - VLowStress,SlowAtten	Kotha et al., 2020 - MidStress,SlowAtten	Kotha et al., 2020 - VHighStress,SlowAtten
Kotha et al., 2020 - LowStress,FastAtten	Kotha et al., 2020 - HighStress,FastAtten	Lanzano et al., 2019 + Lanzano et al., 2022
Kotha et al., 2020 - LowStress,MidAtten	Kotha et al., 2020 - HighStress,MidAtten	Lanzano et al., 2019
Kotha et al., 2020 - LowStress,SlowAtten	Kotha et al., 2020 - HighStress,SlowAtten	

Figure 11: Trellis plots to compare the scaling with distance of the GMM logic tree branch models. The plots are for Mw 5.0 (top row), 6.0 (middle row), and 7.0 (bottom row), and for the ground motion intensity measures of PGA (left column), SA(0.2 s) (centre column) and SA(1.0 s) (right column), respectively. All plots show acceleration (g) vs. Rrup (km), which is the closest distance to the rupture plane. The alternative Kotha et al., (2020) stress parameters are plotted in different colours, and the alternative anelastic attenuation in different line types: dashed line = fast attenuation, solid line = mid attenuation, and dotted line = slow attenuation. The Lanzano et al., (2019) model with the reference rock correction factor of Lanzano et al., (2022) is shown as a solid black line. The original Lanzano et al., (2019) model without the correction factor is also plotted (black dashed line) for comparison.

In order to describe the amount of epistemic uncertainty used for the selected GMMs, trellis plots were produced for relevant magnitudes, distances and intensity measures (Figure 11). It can be seen in Figure 11 that the Kotha et al., (2020) alternative anelastic attenuation branches have significantly less of an effect than the alternative stress parameter logic tree branches. Additionally, the Lanzano et al., (2019) with the reference rock correction factor of Lanzano et al., (2022) generally estimates acceleration in the low ranges of Kotha et al., (2020). For the case study site, the reference rock correction factor of Lanzano et al., (2022) lowers the estimated acceleration of Lanzano et al., (2019).

4. Seismic hazard results

In this PSHA for the METIS case study site, a full-path enumeration of the 4,374 logic tree branches was conducted. A weighted-mean hazard curve was then computed from the individual realisations hazard curves for the intensity measures of peak ground acceleration (PGA) and 0.2 s and 1.0 s spectral acceleration (Figure 12), as well as uniform hazard spectra (UHS) (Figure 13) and conditional spectra (CS) (Figure 14).

4.1.   Hazard curves and uniform hazard spectra
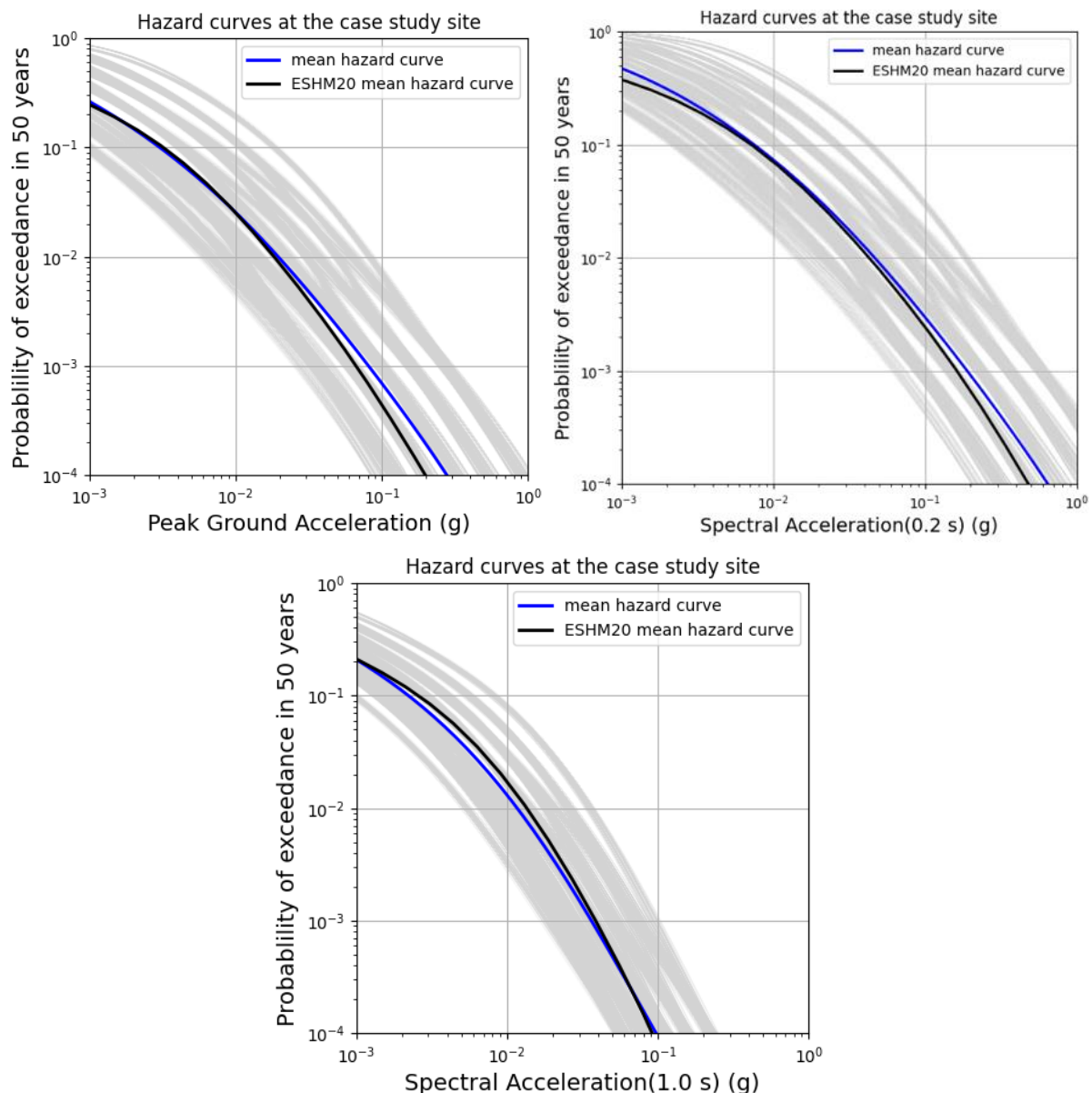

Figure 12: Hazard curves for PGA, SA(0.2 s) , and SA(1.0 s) at the case study site. The mean hazard curve is shown in blue and the individual realisations in grey. The ESHM20 mean hazard curve for the case study site is shown in black.

The uncertainties in the seismogenic-source characterisation included in the logic tree (Figure 10) led to a moderate variability of the result for this site (Figure 12). The main source of uncertainty, however, is associated with the choice of GMM and its uncertainty (Figure 11). Our GMM selection considers the findings of the research described in the METIS Deliverable D4.3 and particularly the section describing the comparison between simulated time-histories with an EGF approach, recordings and empirical ground-motion models.

A UHS was calculated for an equal probability of exceedance for all spectral periods. Specifically, an annual probability of exceedance of 0.001 (1,000 years return period) and then 0.0001 (10,000 years return period) were investigated (Figure 13). It can be seen in Figure 13 that both the ground accelerations and the uncertainty about this acceleration is greater for the lower probability of exceedance. Moderate earthquakes at short distances control the UHS at short periods, and large far away earthquakes control the UHS at long periods.

A CS, with conditional mean and conditional standard deviation, was calculated for a given spectral acceleration period integrating contributions from the ruptures in all realizations admitted by the hazard model logic tree (Lin et al., 2013). The analysis was conducted for a spectral acceleration at a period of 0.2 s and for an annual probability of exceedance of 0.001 (1,000 years return period) and then 0.0001 (10,000 years return period) using the cross-correlation model of Baker and Jayaram (2008) (Figure 14).
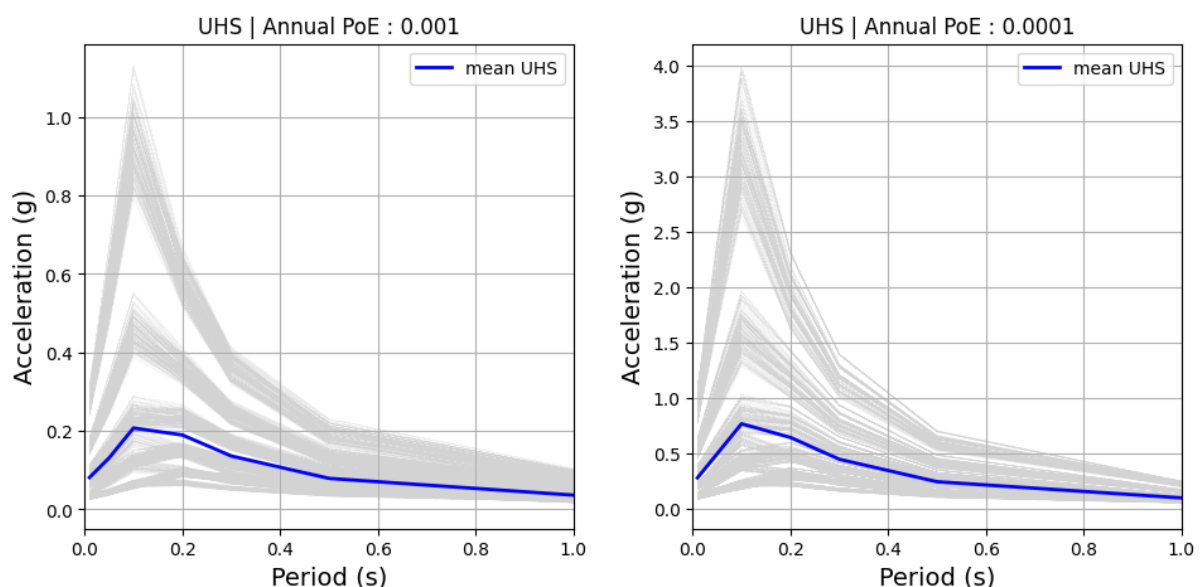
Figure 13: Uniform hazard spectra (UHS) for the case study site. The response spectra are shown for an annual probability of exceedance of 0.001 (1,000 years return period) and 0.0001 (10,000 years return period). The mean UHS is shown in blue, and they grey lines are the individual realizations.
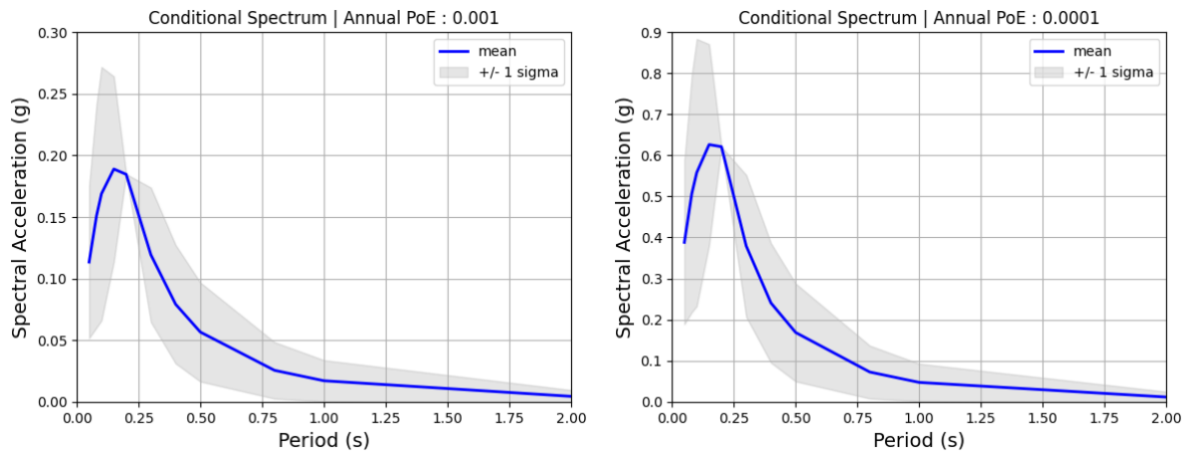
Figure 14: Conditional spectrum for the case study site for the spectral acceleration at a period of 0.2 s. The probability distribution of spectral acceleration over a range of periods is shown for an annual probability of exceedance of 0.001 (1,000 years return period) (left) and 0.0001 (10,000 years return period) (right). The blue line is the mean spectrum and the light grey shaded area is the standard deviation about the mean.

4.2.   Hazard disaggregation analysis

Seismic hazard disaggregation was conducted to determine the relative contribution of ruptures corresponding to various magnitude and distance combinations to the total hazard computed for the case study site. Specifically, the disaggregation of the total hazard into magnitude and distance bins allows the dominant scenario earthquake to be identified.

The contribution to hazard at the site for a 10% probability of exceedance over 50 years is spread out over a large distance with significant participation from ruptures to up to 40 km for PGA and 80 km for SA(1.0 s) (Figure 15). However, these are from very low level of acceleration (Figure 11). For 0.5% probability of exceedance over 50 years (return period 10,000 years), which is commonly used for nuclear design applications, the contribution to the hazard is concentrated within 20 km for PGA and 40 km for SA(1.0 s). For PGA, moderate magnitude earthquakes occurring more often, are contributing to the hazard. For SA(1.0 s) larger magnitude earthquakes, with larger rupture areas, are contributing to the hazard.
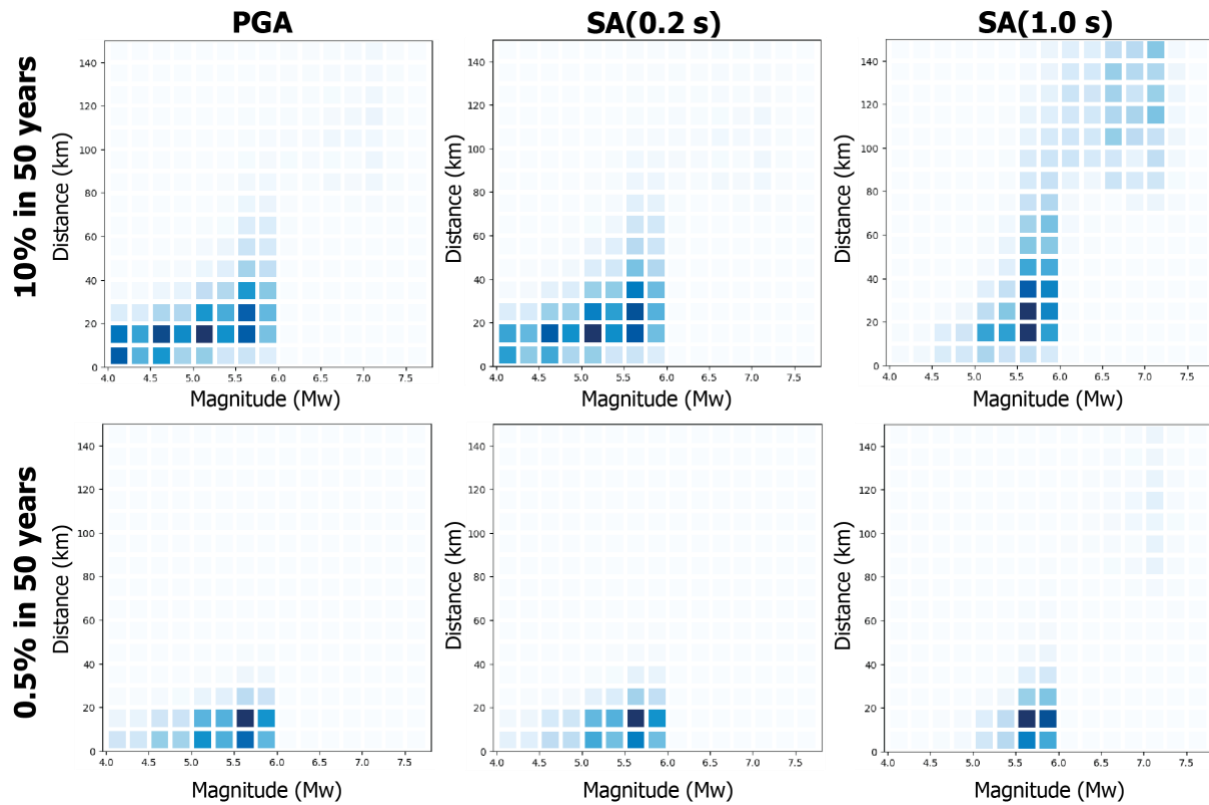
Figure 15: Hazard disaggregation for the intensity measures PGA, SA(0.2 s), and SA(1.0 s) at a 10 % and 0.5 % probability of exceedance over 50 years.
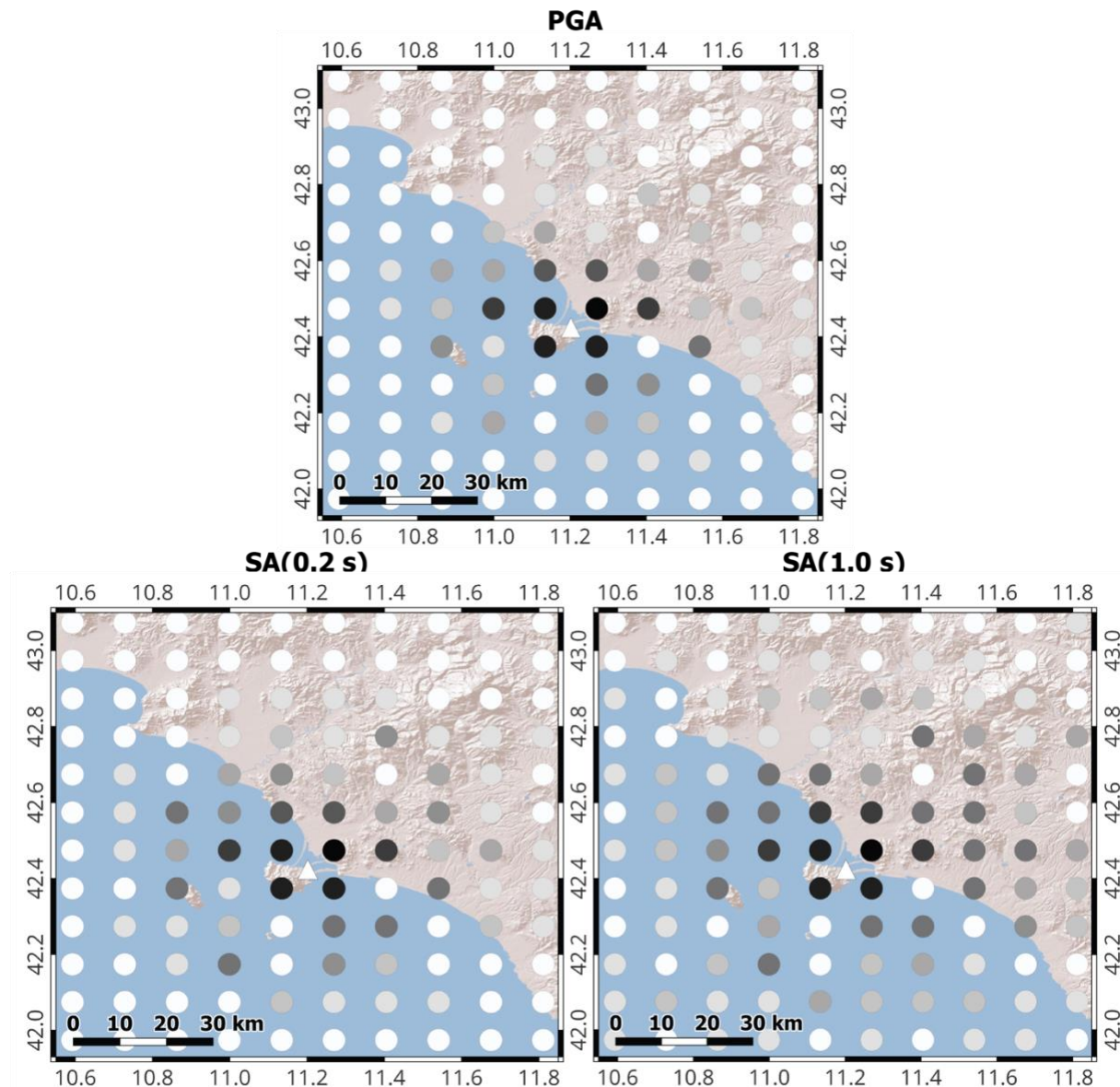
Figure 16: Disaggregation in longitude and latitude around the case study site (white triangle) for a probability of exceedance of 0.5% in 50 years for PGA, SA(0.2 s), and SA(1.0 s). The darkness of the colour of the points represents the contribution to the hazard of each latitude-longitude bin.

Finally, a geographical disaggregation of the seismic hazard results was conducted to identify the location of the highest rupture participation rate for the METIS case study site. This geographical disaggregation showed that the most important sources for the hazard at the METIS case study site are located onshore and near the site (Figure 16). This is consistent with the pattern of the smoothed seismicity shown in Figure 9.

5. Supplementary materials

The OQ Engine input model described in this report is available on the GEM cloud. (https://cloud.openquake.org/s/XZo2iTeTGnWnG8F).

6. References

Baker, J. W., Jayaram N. (2008). Correlation of Spectral Acceleration Values from NGA Ground Motion Models. Earthquake Spectra, 24(1), 299-317. https://doi:10.1193/1.2857544

CEN (2004). Eurocode 8. Design of Structures for Earthquake Resistance—Part 1: General Rules Seismic Actions and Rules for Buildings, EN 1998-1.

Chartier, T. (2022). Seismic source characterisations methodologies and applications. Deliverable 4.1, METIS project, 30 pages.

Danciu L., Nandan S., Reyes C., Basili R., Weatherill G., Beauval C., Rovida A., Vilanova S., Sesetyan K., Bard P-Y., Cotton F., Wiemer S., Giardini D. (2021). The 2020 update of the European Seismic Hazard Model: Model Overview. EFEHR Technical Report 001, v1.0.0. https://doi.org/10.12686/a15

DISS Working Group (2021). Database of Individual Seismogenic Sources (DISS), Version 3.3.0: A compilation of potential sources for earthquakes larger than M 5.5 in Italy and surrounding areas. Istituto Nazionale di Geofisica e Vulcanologia (INGV). https://doi.org/10.13127/diss3.3.0

Frankel, A., (1995). Mapping Seismic Hazard in the Central and Eastern United States. Seismological Research Letters 66, 8–21. https://doi.org/10.1785/gssrl.66.4.8

Gardner, J. K., Knopoff, L. (1974). Is the sequence of earthquakes in Southern California, with aftershocks removed, Poissonian? Bulletin of the Seismological Society of America, 64(5), 1363-1367. https://doi.org/10.1785/BSSA0640051363

Grünthal, G. (1985). The up-dated earthquake catalogue for the German Democratic Republic and adjacent areas-statistical data characteristics and conclusions for hazard assessment." 3rd International Symposium on the Analysis of Seismicity and on Seismic Risk, Liblice/Czechoslovakia, 17–22 June 1985 (Proceedings Vol. I, 19–25)

Kotha, S.R., Weatherill, G., Bindi, D., Cotton, F. (2020). A regionally-adaptable ground-motion model for shallow crustal earthquakes in Europe. Bull Earthquake Eng 18, 4091–4125. https://doi.org/10.1007/s10518-020-00869-1

Lanzano, G., Felicetta, C., Pacor, F., Spallarossa, D., Traversa, P. (2020). Methodology to identify the reference rock sites in regions of medium-to-high seismicity: an application in Central Italy, Geophysical Journal International, 222(3), 2053–2067. https://doi.org/10.1093/gji/ggaa261

Lanzano, G., C. Felicetta, F. Pacor, D. Spallarossa, and P. Traversa (2022). Generic-To-Reference Rock Scaling Factors for Seismic Ground Motion in Italy, Bull. Seismol. Soc. Am. 112, 1583–1606, https://doi.org/10.1785/0120210063

Leonard, M. (2014). Self-consistent earthquake fault-scaling relations: Update and extension to stable continental strike-slip faults. Bulletin of the Seismological Society of America, 104(6), 2953-2965. https://doi.org/10.1785/0120140087

Lin, T., Harmsen, S. C., Baker, J. W., Luco, N. (2013). Conditional Spectrum Computation Incorporating Multiple Causal Earthquakes and Ground-Motion Prediction Models. Bulletin of the Seismological Society of America, 103(2A), 1103–1116. https://doi.org/10.1785/0120110293

Lolli B., Randazzo D., Vannucci G., Gasperini P. (2020). The Homogenized Instrumental Seismic Catalog (HORUS) of Italy from 1960 to Present. Seismological Research Letters, 91(6), 3208–3222. https://doi.org/10.1785/0220200148.

Pagani, M., Monelli, D., Weatherill, G., Danciu, L., Crowley, H., Silva, V., Henshaw, P., Butler, L., Nastasi, M., Panzeri, L., Simionato, M., Viganò, D. (2014). OpenQuake Engine: An Open Hazard (and Risk) Software for the Global Earthquake Model. Seismological Research Letters, 85, 692-702. https://doi.org/10.1785/0220130087

Rovida A., Locati M., Camassi R., Lolli B., Gasperini P., Antonucci A. (eds), 2022. Italian Parametric Earthquake Catalogue (CPTI15), version 4.0. Istituto Nazionale di Geofisica e Vulcanologia (INGV). https://doi.org/10.13127/CPTI/CPTI15.4

SSHAC (Senior Seismic Hazard Analysis Committee). (1997). Recommendations for Probabilistic Seismic Hazard Analysis: Guidance on Uncertainty and Use of Experts. Retrieved from https://www.nrc.gov/docs/ML0800/ML080090003.pdf

SSHAC (Senior Seismic Hazard Analysis Committee). (2012). Practical Implementation Guidelines for SSHAC Level 3 and 4 Hazard Studies. Retrieved from https://www.nrc.gov/docs/ML1211/ML12118A445.pdf

Uhrhammer, R. A. (1986). Characteristics of northern and central California seismicity. Earthquake Notes 57(1) 21.

Visini, F., Meletti, C., Rovida, A., D'Amico, V., Pace, B. Pondrelli, S. (2022). An updated area-source seismogenic model (MA4) for seismic hazard of Italy. Nat. Hazards Earth Syst. Sci., 22, 2807–2827. https://doi.org/10.5194/nhess-22-2807-2022

Weatherill, G., Kotha, S. R. and Cotton, F. (2020). A regionally-adaptable 'scaled-backbone' ground motion logic tree for shallow seismicity in Europe: application to the 2020 European seismic hazard model. Bulletin of Earthquake Engineering, 18, 5087 – 5117. https://doi.org/10.1007/s10518-020-00899-9

Weichert, D.H. (1980) Estimation of the earthquake recurrence parameters for unequal observation periods for different magnitudes. Bulletin of the Seismological Society of America, 70, 1337-1346. https://doi.org/10.1785/BSSA0700041337

7. Appendix A

We provide in this appendix some additional plots of the magnitude-frequency distributions computed for some of the sources at closest distance to the investigated site.